

# 低压电弧喷涂涂层组织及其后处理工艺

李德元, 宋 丹, 张忠礼, 赵灵艳

(沈阳工业大学 材料科学与工程学院, 沈阳 110178)

**摘 要:** 采用4Cr13、铝和钛喷涂丝材分别在大气环境和低度真空环境中制备了喷涂层。通过金相组织分析和定点成分分析对比了涂层的组织形态、化合物的数量及分布状态; 并通过加压试验分析了涂层在压力作用下, 涂层内部孔隙弥合的情况; 最后通过加热使涂层组织中发生再结晶, 研究了再结晶处理对涂层组织的影响。结果表明, 低压电弧喷涂可以有效地减少4Cr13和铝涂层中的氧化物数量, 且通过加压及再结晶处理可以使涂层粒子间形成冶金结合。但对于钛涂层, 所提供的低压喷涂环境还不能提供很有效的防护, 再结晶处理也无法获得粒子间良好的冶金结合。

**关键词:** 电弧喷涂; 涂层; 喷涂粒子; 氧化物; 再结晶

**中图分类号:** TG115.28 **文献标识码:** A **文章编号:** 0253-360X(2009)04-0001-04



李德元

## 0 序 言

1990年, 德国Steffens等人<sup>[1]</sup>采用低压等离子喷涂方法成功地制备了具有极低氧化物含量的钛涂层。Brzezinski等人<sup>[2,3]</sup>则用低压等离子喷涂制备了热障涂层。这项技术还被用于复合材料涂层和生物医学材料涂层制备, 获得了良好的效果<sup>[4,5]</sup>。由于低压等离子喷涂用粉末作为喷涂材料, 粉末的比表面积很大, 要去除粉末表面吸附的气体难度较大。线材的比表面积较小, 而且价格便宜, 因此又出现了低压电弧喷涂技术, 并被用于钛、钽一类对氧和氮极其敏感材料涂层的制备<sup>[6]</sup>。

采用低压电弧喷涂方法制备了4Cr13、铝和钛涂层, 分析了这些涂层的组织特征, 并研究了加压和再结晶等后处理工艺对涂层组织结构的影响, 为进一步推广这种工艺提供了一些相关的数据。

## 1 试验方法

低压电弧喷涂所需要的低度真空环境由真空泵提供, 在喷涂前预先将真空室的压力抽至10 Pa。电弧喷涂的主要工艺参数为: 喷涂电压35 V; 喷涂电流140 A; 喷涂距离150 mm, 雾化气体为氩气, 气体压力0.3 MPa。

喷涂试件的尺寸为20 mm×20 mm×5 mm; 涂层厚度为2 mm; 基体材料为Q235低碳钢, 喷涂丝材分别选用4Cr13、纯铝和纯钛丝。

喷涂后对涂层试样进行了后处理, 首先对试样进行了静载加压, 其目的是为了为了使喷涂时形成的孔隙弥合。考虑到各种涂层材料屈服极限的不同, 对于4Cr13、铝和钛涂层, 所施加的压力分别为720, 100和500 MPa。又对加压后的试件进行了加热, 以研究再结晶过程对涂层组织的影响。加热在真空热处理炉中进行, 考虑到各种涂层材料再结晶温度的不同, 对于4Cr13、铝和钛涂层, 分别加热到650, 330, 600 °C, 保温1 h。

## 2 试验结果及分析

### 2.1 4Cr13 涂层

图1是在大气中进行喷涂后所得到的4Cr13涂层的组织。利用能谱分析对涂层不同部位进行成分分析, 结果表明在大气喷涂的条件下, 涂层中的氧化物主要分布在扁平化粒子间的交界部位。如图中点2处氧元素的质量分数达到24.34%, 而扁平化粒子内部点1处氧元素则仅为1.52%, 在涂层组织照片中可见, 氧化物呈暗灰色, 主要分布于粒子的边界处。

图2是低压喷涂条件下所获得的4Cr13涂层的组织。由图中可以看出, 粒子边界处不再出现灰色的氧化物层。对喷涂粒子内部点1和粒子界面处点2进

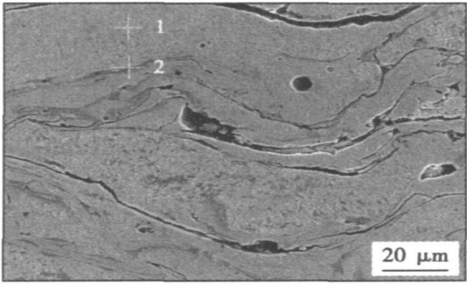


图 1 大气喷涂 4Cr13 的涂层组织

Fig. 1 Microstructure of 4Cr13 coatings sprayed in air

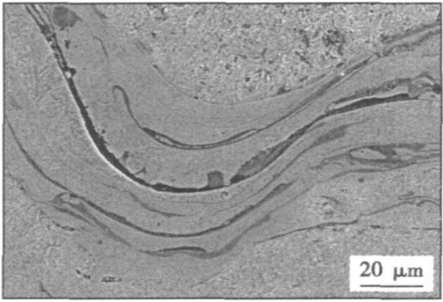


图 3 热处理后的大气喷涂 4Cr13 涂层组织

Fig. 3 Microstructure of 4Cr13 coatings sprayed in air after heat treatment

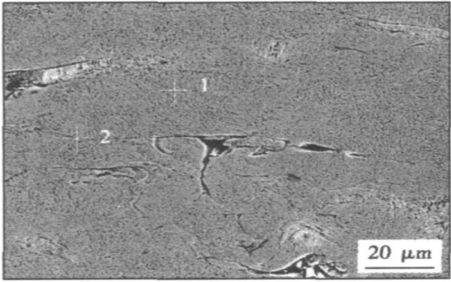


图 2 低压喷涂 4Cr13 的涂层组织

Fig. 2 Microstructure of 4Cr13 coatings sprayed in low pressure condition

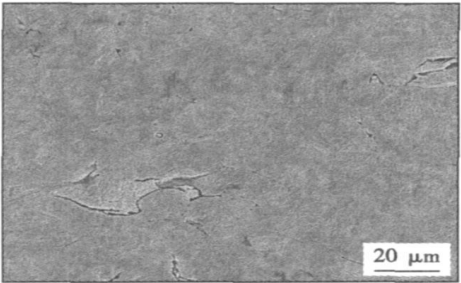


图 4 热处理后的低压喷涂 4Cr13 涂层组织

Fig. 4 Microstructure of 4Cr13 coatings sprayed in low pressure condition after heat treatment

由以上的对比可以看出, 采用低压电弧喷涂可以有效地防止 4Cr13 涂层氧化, 但涂层组织中仍可以明显地看到粒子之间的边界, 且存在一定量的孔隙. 在喷涂状态下, 粒子中的马氏体片还不能穿越粒子边界形成冶金结合.

为了探讨在喷涂粒子间形成冶金结合的途径, 分别对大气电弧喷涂和低压电弧喷涂所获得的 4Cr13 涂层进行了静载加压, 所施加的静载压力为 720 MPa, 然后在真空热处理炉中加热至 650 ℃. 图 3 是大气喷涂涂层的组织变化情况. 由图中可见, 通过加压处理后, 部分孔隙得到了弥合, 但由于氧化物存在的区域具有一定的厚度, 在热处理后, 虽然扁平化粒子内部的晶粒组织形态也发生了变化, 但无法越过氧化物层在粒子间形成冶金结合.

图 4 是经过加热后的低压喷涂涂层的组织形态. 由图中可以看出, 经过在再结晶温度区的加热后, 马氏体组织发生了再结晶, 形成了上贝氏体组织, 其晶粒已经穿越大多数粒子边界, 形成了良好的

冶金结合. 但加压还无法完全使粒子之间的孔隙弥合, 在粒子边界的有些部分仍然存在不连续的部位.

试验表明, 当采用低压电弧喷涂对 4Cr13 钢基体材料进行喷涂时, 由于材料本身氧化倾向不十分强烈, 因此基本上可以防止涂层的氧化. 如果对此种涂层进行滚压等塑性变形处理, 并在再结晶温度区进行加热和保温, 就可以获得喷涂粒子之间的冶金结合. 另外, 需要说明的是在低压电弧喷涂条件下, 除了低度真空的作用外, 以氩气作为雾化气体对于减少氧化物也是有一定作用的.

2.2 铝涂层

试验研究发现, 低压电弧喷涂和大气中喷涂的铝涂层在组织形态上差别并不明显, 但大气喷涂组织中含有更多数量的氧化物夹杂. 图 5 是在大气喷涂条件下, 存在于两个扁平化粒子之间的一个夹杂物的形貌. 对该夹杂物进行能谱分析表明该处富集了大量的氧, 氧与铝的摩尔分数分别占 62.77% 和 37.23%, 与  $Al_2O_3$  的摩尔分数接近.

图 6 是低压电弧喷涂所获得的铝涂层组织, 组织中同样也有一定数量的孔隙存在, 对此处进行能谱分析的结果表明, 此处氧与铝的摩尔分数分别占 15.80% 和 84.20%, 说明此处  $Al_2O_3$  含量明显少于大

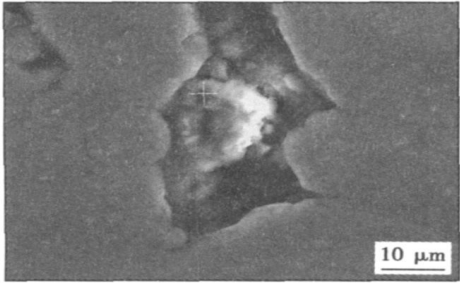


图 5 大气喷涂铝涂层中的夹杂物

Fig. 5 An inclusion in Al coatings sprayed in air

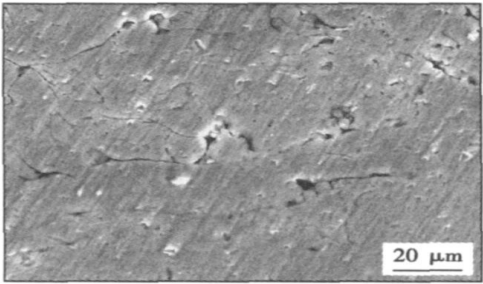


图 8 热处理后的低压喷涂铝涂层组织

Fig. 8 Microstructure of Al coatings sprayed in low pressure condition after heat treatment

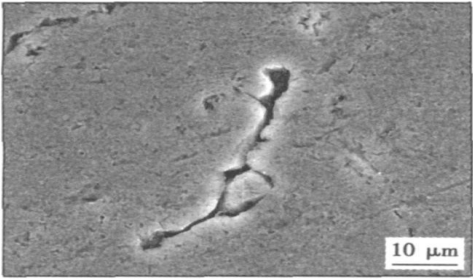


图 6 低压喷涂铝涂层中的夹杂物

Fig. 6 An inclusion in Al coatings sprayed in low pressure condition

气中喷涂的情况。

图 7 是对低压电弧喷涂的铝涂层加压后的组织。由图中可见, 原来的孔隙在加压后已经大部分弥合。将加压后的涂层加热到 330 °C, 并保温 1 h 后的组织如图 8 所示。由图中可见, 铝晶粒明显长大, 有些扁平化粒子边界已经消失, 形成了冶金结合。但涂层中仍然有一些孔隙存在, 再结晶晶粒无法穿过这些未弥合的孔隙。

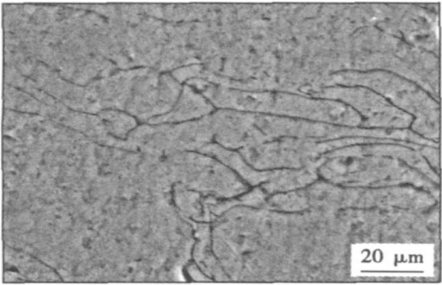


图 7 加压后的低压喷涂铝涂层组织

Fig. 7 Microstructure of Al coatings sprayed in low pressure condition after being pressed

2.3 钛涂层

试验表明, 如果采用压缩空气作为雾化气体, 很

难完成钛的电弧喷涂。为了与低压电弧喷涂进行比较, 在试验中采用氩气作为雾化气流, 在大气环境中进行了喷涂, 所获得的涂层组织如图 9 所示。由图中可以看出, 此时仍然不能形成组织致密的涂层, 由于钛极易被空气中的氧和氮所污染, 因此喷涂粒子甚至无法顺利地完 成扁平化的过程, 呈大颗粒堆积, 颗粒之间则夹有不规则形状的夹杂物。采用能谱分析对图中夹杂物进行成分分析的结果表明, 氮的摩尔分数为 22.86%, 而氧的摩尔分数为 11.02%, 说明该处含有大量的氮化物和氧化物, 且氮化物含量更高一些。

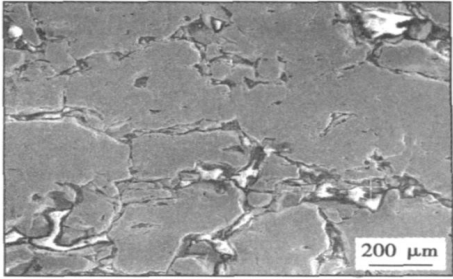


图 9 大气喷涂钛涂层的组织

Fig. 9 Microstructure of Ti coatings sprayed in air

图 10 是低压电弧喷涂条件下所获得的钛涂层的组织, 由图中可以看出, 此时夹杂物仍然存在, 但大多已经变得很细小, 在组织中弥散分布, 主要分布于喷涂粒子的边界处。由图中可以明显看到扁平化粒子的形态, 粗大的颗粒已不再出现。对图中呈链状分布的夹杂物颗粒进行能谱分析, 所获得的结果表明, 此处氮的摩尔分数为 5.67%, 氧的摩尔分数为 1.17%, 比大气喷涂时要少得多。此处氧含量已经与粒子内部的含量相近, 说明此处不再存在氧化物的富集, 但氮含量仍明显高于粒子内部, 说明此处

仍然有氮化物存在.

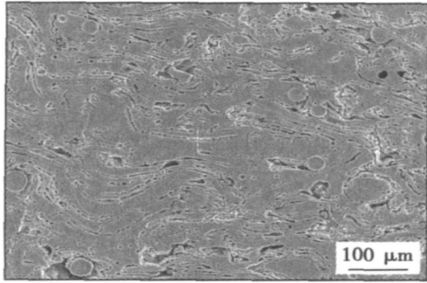


图 10 低压喷涂钛的涂层组织

Fig. 10 Microstructure of Ti coatings sprayed in low pressure condition

比较图 9 和图 10 可见,在大气环境下,很难获得致密的钛涂层,这是由于喷涂粒子在飞行过程中已经被空气中的氮和氧严重污染,在粒子表面形成一定厚度的化合物层.由于这些化合物的熔点都比较高,所以在粒子撞击到基体时它们已经凝固,并具有一定强度,造成粒子扁平化过程无法正常完成,形成了大颗粒粒子与夹杂物层堆积在一起的混杂组织.而在低压电弧喷涂的低度真空环境中,喷涂粒子的污染程度明显降低,氧化物和氮化物的数量也显著减少,所以不再影响到粒子的扁平化过程.但由于在文中试验所提供的真空度下,仍然无法对喷涂粒子形成十分可靠的保护,因此仍然有少量的氮化物和氧化物形成,这些化合物零散地分布于扁平化粒子的交界处,形成“细链”状的组织.

对低压喷涂所获得的钛涂层进行加压和再结晶处理.结果表明,虽然在个别部位可以看到再结晶晶粒穿过粒子边界的情况,但由于边界上有大量夹杂物存在,粒子之间基本上还是处于非连续的状态.

### 3 结 论

(1) 采用低压电弧喷涂制备了 4Cr13、铝和钛涂

层.组织和成分分析结果表明,该种喷涂工艺可以显著降低涂层中的氧化物和氮化物含量,但对涂层中孔隙的数量没有明显影响.

(2) 对于低压电弧喷涂的 4Cr13 和铝涂层,由于扁平化粒子边界处的氧化物数量较少,通过加压和再结晶等后处理工艺后,再结晶晶粒可以穿越粒子边界形成冶金结合.

(3) 利用低压电弧喷涂钛涂层时,虽然可以使喷涂粒子得到一定程度的保护,但涂层中仍存在一定的氮化物,此时,采用加压和加热等后处理工艺也难以在涂层中获得良好的冶金结合.

### 参考文献:

- [1] Steffens H D, Dvorak M. Structure and electrochemical behavior of vacuum-plasma sprayed titanium and plasma-beam alloyed titanium coatings[C] // 3rd National Thermal Spray Conference, California, 1990: 207—210.
- [2] Brzezinski T, Cavasin A. Vacuum sprayed  $ZrO_2$  barrier coatings for aerospace application[C] // 15th International Thermal Spray Conference, France, 1998: 1645—1650.
- [3] Gruner H. Vacuum sprayed composite coatings[C] // 11th International Thermal Spraying Conference, Canada, 1986: 73—82.
- [4] 郑学斌, 季 珩, 丁传贤, 等. 真空等离子喷涂抗菌 HA 涂层研究[J]. 生物骨科材料与临床研究, 2005, 2(5): 7—10.  
Zheng Xuebin, Ji Heng, Ding Chuangxian, *et al.* Study on the HA coatings prepared by vacuum plasma spraying[J]. Orthopaedic Biomechanics Materials and Clinical Study, 2005, 2(5): 7—10.
- [5] Zhao L, Lugscheider E. Reactive plasma spraying of TiAl6V4 alloy[J]. *Weare*, 2002, 253(11—12): 1214—1218.
- [6] Steffens H D, Wewel M. Vacuum arc spraying—an advanced coating technology[C] // 12th International Thermal Spraying Conference, London, 1989: 61—63.

作者简介: 李德元,男,1959 年出生,博士,教授,博士生导师.主要从事焊接工艺与设备、表面强化技术方面的科研和教学工作.发表论文 70 余篇.

Email: dny1962@sina.com

## MAIN TOPICS, ABSTRACTS & KEY WORDS

### Study on microstructure of the coatings sprayed in low pressure condition and its post treatment technology

LI Deyuan,

SONG Dan, ZHANG Zhongli, ZHAO Lingyan (School of Materials Science and Engineering, Shenyang University of Technology, Shenyang 110178, China). p1-4

**Abstract:** In order to make clear the effect of the spraying technology on the coatings microstructure formation in the low pressure spraying, the wires of 4Cr13, Al and Ti were adopted to prepare the spraying coatings in air and low pressure condition, respectively. The microstructure, the amount of the compounds and their distribution pattern in both coatings were compared by the microanalysis and micro-area chemical analysis. Static press test was used to investigate the closing possibility of the porosities. After the press test, the coatings were heated to certain temperature to analyze the effect of the recrystallization heat treatment on the coatings microstructure. As a result, the amount of the oxide in 4Cr13 and Al coatings has been reduced obviously in the low pressure condition, and metallurgy combination between the splat particles can be formed by pressing and heating. However the low pressure condition can not provide sufficient protection for the Ti coatings, the following recrystallization heat treatment can not get metallurgy combination between the particles.

**Key words:** arc spraying; coatings; spraying particle; oxide; recrystallization

### Full digital control of $I/I$ mode pulsed MIG welding based on triple closed loop control

SHA Deshang, Liao Xiaozhong

(School of Automation, Beijing Institute of Technology, Beijing 100081, China). p5-7, 12

**Abstract:** This paper presents a full digital control strategy for pulsed MIG/MAG welding based on digital signal processor (DSP) control. One droplet per one pulse (ODPP) is maintained with the proposed control strategy which is characterized by  $I/I$  mode with adaptive voltage compensation (AVC). Welding database with different materials and diameters is established according to wire feed speed. Arc length is detected during each pulse period and the melting rate is changed. Moreover, real time compensation for the volt drop across the wire stickout is made to ensure the arc length constant while stickout changing. Operation principles are analyzed and control block diagram composed of triple closed loop is also presented. Experimental results show that the proposed method is feasible and universal. Constant arc length is realized when wire stickout changes. The welding process is stable and the welding bead is also good with the proposed method.

**Key words:** pulsed MIG welding; full digital control; arc length

### Stereovision-based detection of 3-D weld seam using epipolar line constraint and laser stripe indication

LI Hexi<sup>1,2</sup>, WANG

Guorong<sup>1</sup>, SHI Yonghua<sup>1</sup>, ZHANG Weimin<sup>1</sup> (1. College of Mechanical and Automotive Engineering, South China University of Technology, Guangzhou 510640, China; 2. College of Information Engineering, Wuyi University, Jiangmen 529020, Guangdong, China). p8-12

**Abstract:** An epipolar line constraint equation is established for a binocular stereovision system mounted at the end-effector of welding robot. The stereovision correspondence technique based on the combination of epipolar line constraint with laser stripe indication is applied to detect the position of a three-dimensional (3-D) saddle-shaped weld seam which is produced by the intersection of two circular pipes. The experimental results show that the smooth segments of laser stripe in the weld seam image can be obtained using thinning and deburring arithmetics, and the stereovision correspondences between pairs of points at the left and the right images can be dependably realized by detecting both the singular points of laser stripe curvature and the intersecting points of laser stripe with epipolar line, thus the detection accuracy to the 3-D weld seam and its adjacent area can be improved. The geometrical shape of the 3-D weld seam is reconstructed from the 3-D data acquired by stereovision-based detection with less errors compared with its actual dimension, therefore the proposed method can satisfy the detection requirement of 3-D weld seam in automatic robot welding system.

**Key words:** stereovision; epipolar line constraint; laser stripe indication; correspondence; weld seam detection

### Plasma component calculation in underwater wet welding

LI

Zhigang, ZHANG Hua, JIA Jianping (Institute of Mechatronics Engineering, Nanchang University, Nanchang 330031, China). p13-16

**Abstract:** The electric arc is formed in the ionized gas bubble in the underwater wet welding. Combined with the previous bubbles components determination, the main ionization and dissociation process in the bubble are analyzed. The calculation based on the potapov model was done for the underwater arc components at different water pressures and temperatures under the local thermodynamics equilibrium state. Its main theoretical bases are the Dalton law of partial pressure, the law of mass action, the electric charge quasi-neutrality condition and the chemistry measurement equilibrium condition. The results show that with the pressure increasing from 0.1013 MPa to 1.013 MPa and then to 10.13 MPa, the density of H, H<sup>+</sup>, O, C, O<sup>+</sup>, C<sup>+</sup> is increased, but the average ionization degree is not influenced by the water pressure.

**Key words:** underwater wet welding; electric arc; components calculation

### Recognition and positioning of start welding position for arc welding robot

CHEN Xizhang<sup>1</sup>, CHEN Shanben<sup>2</sup>

(1. School of Material Science and Engineering, Jiangsu University, Zhenjiang